EPJ manuscript No.
(will be inserted by the editor)

Polarimetry of small bodies and satellites of our Solar System

S. Bagnulo[1], I. Belskaya[2], A. Cellino[3], and L. Kolokolova[4]

[1] Armagh Observatory and Planetarium, College Hill, Armagh BT61 9DG, UK. Email: sba@arm.ac.uk
[2] Institute of Astronomy, V.N. Karazin Kharkiv National University, 35 Sumska str., 61022 Kharkiv, Ukraine. Email: irina@astron.kharkov.ua
[3] INAF - Osservatorio Astrofisico di Torino, I-10025 Pino Torinese, Italy. Email: cellino@oato.inaf.it
[4] University of Maryland, College Park, MD, United States. Email: lkolokol@umd.edu

Received: 5 May 2017 / Revised version: date

Abstract. The large majority of astronomical observations are based on intensity measurements, either as a function of wavelength, or time, or both. Polarimetry, a technique which measures the way in which the electromagnetic field associated to the radiation oscillates, does provide further information about the objects that have emitted or scattered the observed radiation. For instance, polarimetric measurements can provide important constraints to the characterisation of the cosmic dust (be it of interstellar or cometary origin) of the surfaces of the atmosphereless bodies, and of planetary atmospheres. This property has been exploited in solar system science to study asteroids, comets, rocky and giant gaseous planets, and their satellites. In this paper we present a review of the polarimetric studies of the small bodies of the solar system.

PACS. PACS-key describing text of that key – PACS-key describing text of that key

1 Introduction

Scattered light is partially polarized, in a way that depends on the properties of the scatterers and on the angle between the incident and scattered light. This may be understood in a schematic way by thinking of an electron on a given surface being hit by the incoming radiation at a non-zero incidence angle. As sketched in Fig. 1, this produces an oscillation of the electron, which is less free to penetrate the medium than it is to move in a direction parallel to the surface. Therefore, the emerging light has an excess of linear polarization oriented along the scattering surface, and perpendicular to the scattering plane (which is the plane defined by the incident and the emerging radiation).

When measuring scattered light, it is common practice to define the Stokes Q and U parameters adopting as a reference direction the direction perpendicular to the scattering plane. This way, Stokes Q is proportional to the component of the electric field associated to the radiation perpendicular to the scattering plane minus the component parallel to it (both components are perpendicular to the direction of propagation of the light), and is expected to be positive. For symmetric reasons, Stokes U is expected to be zero. Fresnel laws tell us that the amount of polarisation of the reflected light depends on the refractive index of the surface and on the angle between the incident light and the reflected light. This may help to understand that, by studying the Stokes parameters of the scattered radiation at different phase-angles (the phase-angle is the angle between the sun, the object, and the observer), one may in principle retrieve information about the surface structure and composition of the scattering body.

Polarimetric observations of the objects of the Solar System may be used to detect molecules and aerosol hazes of planetary atmospheres (and perhaps characterize the underlying planetary surfaces), to characterize the dust in cometary atmospheres or the surfaces of atmosphereless objects such as most of the planet moons and all asteroids. Obviously, theoretical modelling is much more complicated than what sketched above. First of all, the Solar System is not in a laboratory controlled condition. We cannot easily experiment with different angles of incidence of the incoming radiation, but we have to observe targets at different geometrical configurations relative to the Earth during their orbit around the Sun. Most importantly, the properties of the light scattered by the bodies of our Solar System cannot be simply described by a single reflection on a flat surface. To model the surfaces of atmosphereless bodies of the Solar System one has to consider multiple scattering on a surface that is irregular at a microscopic level. Topography of small bodies and their irregular shape also require that the radiation beam received by the observer should be thought

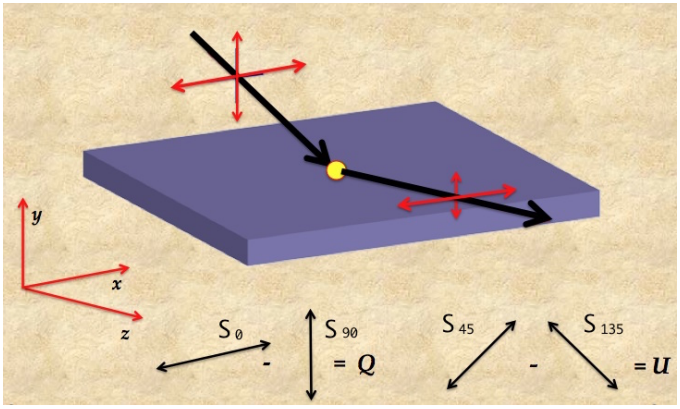

Fig. 1. Polarization of the light reflected by a plane surface. We consider a right handed reference system with the $z-$axis directed along the direction of propagation of the reflected light, and the $x-$axis perpendicular to the scattering plane (the plane containing the incident and the reflected beam). We denote with S_α the signal received through an ideal filter for linear polarization with its acceptance axis oriented at an angle α measured counterclockwise looking at the source, and set to 0° when parallel to the x direction (hence 90° when parallel to the y direction). Stokes Q is proportional to $S_0 - S_{90}$ and Stokes U to $S_{45} - S_{135}$. The quantity P_r defined in Eq. (1) is given by $(S_0 - S_{90})/(S_0 + S_{90})$.

as the superposition of various beams emerging at different scattering angles. For cometary dust, one has to model the complex interaction between the electromagnetic field and irregular or aggregated particles. Practically, while polarimetric measurements of planetary atmospheres and cometary dust may be modelled in some detail, most of the polarimetric observations of atmosphereless bodies of the Solar System are more often used for classification purpose, or for a semi-empirical analysis.

Polarimetric observations of the small bodies of the Solar System, including main-belt asteroids, Jupiter Trojans, Centaurs, trans-Neptunian objects and comets are the subject of this paper. In Sect. 2 we will make a general presentation of the nature of the polarimetric observations of Solar System objects, including some considerations on observing and modelling techniques. The remaning Sections are dedicated to a review of the observations of various categories: main-belt asteroids (Sect. 3), Jupiter Trojans, Centaurs and trans-Neptunian objects (Sect. 4), planetary moons (Sect. 5), and comets (Sect.6). We note that by far, the large majority of polarimetric measurements of Solar System bodies are measurements of *linear* polarization. No convincing detection of circular polarization in asteroids has been reported so far, although claims of detection of circular polarization in the Moon and in comets have been made in the literature (see Sects. 5 and 6). Measurements of circular polarization are particularly challenging because the signal of circular polarization is expected to be very small compared to linear polarization, and are prone to be affected by cross-talk from linear polarization.

2 General characteristics of the observations and their modelling

Polarimetric observations of Solar System objects depend on wavelength and on the phase-angle α. The observer generally reports the quantity P_r defined as the flux perpendicular to the plane Sun-Object-Earth (the scattering plane) minus the flux parallel to that plane, divided by the sum of the two fluxes:

$$P_\mathrm{r} = \frac{I_\perp - I_\parallel}{I_\perp + I_\parallel} \ . \tag{1}$$

By definition, P_r is the reduced Stokes parameter $P_Q = Q/I$ if we adopt as a reference direction the direction perpendicular to the scattering plane (see Fig. 1). For simmetry reasons, for point-source objects the quantity $P_U = U/I$ is expected to be zero and may be used for quality check purpose (see, e.g., Bagnulo et al. 2008, [1]). In practical cases, the observer may decide to physically align the polarimeter to the direction perpendicular to the scattering plane, and measure only P_r. However, a more conservative but more time consuming approach is to always measure both Stokes parameters and verify that $P_U \simeq 0$. We note that observations may be obtained in an arbitrarily oriented reference system S' and then transformed into a system that has the reference direction perpendicular to the scattering plane using the well known transformation formulas (e.g., Landi Degl'Innocenti et al. 2007, [2])

$$\begin{aligned} P_Q &= \ \ \cos(2\chi)\, P_Q{}' + \sin(2\chi)\, P_U{}' \\ P_U &= -\sin(2\chi)\, P_Q{}' + \cos(2\chi)\, P_U{}' \end{aligned} \tag{2}$$

where χ is the angle by which the old S' reference system has to be rotated counterclockwise (looking at the source) to become coincident with the new one. If the observations are obtained with the polarimeter aligned to the great circle passing through the object and the North Celestial Pole (which is a common practice), then $\chi = \Phi + \pi/2$, where Φ is the angle between the direction Object-North Pole and the direction Object-Sun. The angle Φ may be obtained from ephemeris, or derived from the coordinates of the Sun ($\alpha_\odot$,$\delta_\odot$) and of the target ($\alpha_{\rm T}$,$\delta_{\rm T}$) via

$$\sin\delta_{\rm T}\cos(\alpha_\odot - \alpha_{\rm T}) = \cos(\delta_{\rm T})\tan(\delta_\odot) - \sin(\alpha_\odot - \alpha_{\rm T})\frac{1}{\tan(\Phi)} \ .$$

2.1 Broadband polarimetry

The large majority of polarimetric measurements of the objects of the Solar System consists of broadband polarimetric measurements as a function of the phase-angle α:

$$P_{\rm r}(\alpha, X) = \frac{\int_0^{+\infty} {\rm d}\lambda\ T_X(\lambda)\ \left[I_\perp(\lambda,\alpha) - I_\parallel(\lambda,\alpha)\right]}{\int_0^{+\infty} {\rm d}\lambda\ T_X(\lambda)\ \left[I_\perp(\lambda,\alpha) + I_\parallel(\lambda,\alpha)\right]} \ , \tag{3}$$

where $T_X(\lambda)$ is the telescope+instrument transmission function in the filter X. After collecting data at various observing epochs, the observer builds up curves of $P_{\rm r}$ versus α like those shown in Fig. 2. Perhaps the most striking property that can be seen in the plots of Fig. 2 is that at small phase-angles values ($\leq 20°$), we measure a negative value of the polarisation. The term "negative polarization" is probably misleading, as one would naturally think to polarization as a quantity intrinsically positive; this nomenclature is a consequence of the definition of the reference direction adopted for the measurement of the Stokes parameters implicitly assumed in Eq. (1). Negative polarization means that the observed polarization is oriented parallel to the scattering angle, rather than perpendicular to it (as one would expect from the simplified model presented in the previous section), therefore, according to Eq. (1), $P_{\rm r}$ is a negative quantity. This phenomenon was first observed on the Moonshine by Lyot almost a century ago (Lyot 1929, [13]), and since then it has been found ubiquitous in all atmosphereless bodies of the Solar System when observed at small phase-angles.

For surface of atmosphereless bodies, the explanation of this phenomenon probably lies in the mechanism of coherent backscattering (see Sect. 2.5). The phenomenon of negative polarisation is observed also in comets, but its physical explanation must be different, since in cometary coma, single-scattering is the dominant scattering process. In fact, negative polarization may be naturally explained even in the context of ideally spherical particles based on Mie theory (Mukai et al. 1987, [14]).

Polarization curves may be fit by empirical functions. One of the most popular ones is the so-called "trigonometric function" proposed by Lumme & Muinonen (1993) [15]:

$$P_{\rm r}(\alpha) = b\,(\sin\alpha)^{\,c_1}\ \left(\cos\frac{\alpha}{2}\right)^{c_2}\ \sin(\alpha - \alpha_{\rm inv}) \ . \tag{4}$$

As described by Penttilä et al. (2005, [16]), in Eq. (4), the parameter b affects the amplitude of polarization, and its physically meaningful range is between 0 and 1; the parameter $\alpha_{\rm inv}$ is the inversion angle, i.e., the value of the phase-angle at which the polarization curve crosses the zero; the parameter c_1 mainly controls the position of the minimum, while c_2 affects the maximum and the asymmetry of the polarization-phase curve. In case of asteroids, one can also adopt the simplified fitting function introduced by Kaasalainen et al. (2003, [17])

$$P_{\rm r} = A(e^{-\alpha/B} - 1) + C\alpha \ , \tag{5}$$

where the three parameters A, B, C may be determined via a least-square technique (e.g. Cellino et al. 2015a, [18], and references therein). In fact, even simple visual inspection permits us to identify some quantities from the polarization curves: the value of negative polarization $P_{\rm min}$ and the phase-angle value $\alpha_{\rm min}$ at which this occurs, the inversion angle $\alpha_{\rm inv}$, and the slope h of the curve at that point; for objects that can be observed at large phase-angles it is also possible to identify the polarization maximum $P_{\rm max}$ and the phase-angle value $\alpha_{\rm max}$ at which the maximum occurs; these latter quantities can be generally measured only from spacecrafts; from ground-based facilities, they are accessible only for nearby objects, like near-Earth asteroids, comets when approaching the Sun, the Moon, and the planets in inner orbits. In fact, for distant objects, even $\alpha_{\rm inv}$, $\alpha_{\rm min}$ and $P_{\rm min}$ are impossible to measure due to geometrical constraints. If r is the heliocentric distance of the target in au, for the objects orbiting beyond the Earth it is always $\alpha \leq \arcsin(1/r)$; therefore, for main-belt asteroids we typically have $\alpha \lesssim 25°$; for Jupiter and its moons $\alpha \lesssim 11°$; for Pluto and other trans-Neptunian objects $\alpha \lesssim 2°$. Note also that asteroids having high orbital inclinations can be only seldom observed at small phase-angles.

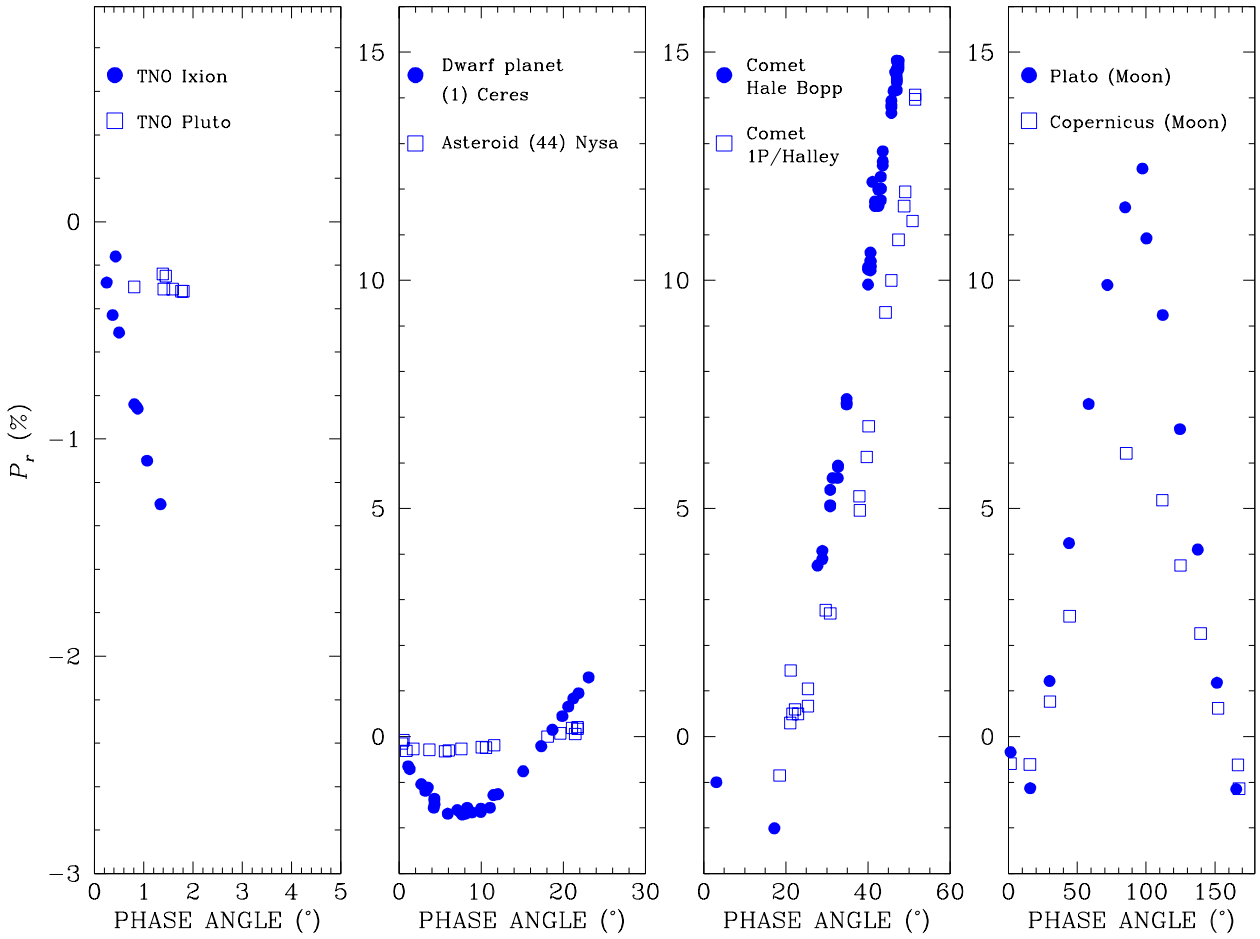

Fig. 2. Broadband polarimetric measurements of various small bodies of the Solar System. Note the different scales adopted for different objects. Observations of TNOs were obtained in the R filter, those of comets in a dust-free band around R, those of asteroids and the Moon in the V and G filters. Data from Boehnhardt et al. (2004,[3]), Breger & Cochran (1982, [4]), Zellner et al. (1974, [5]), Zellner & Gradie (1976b, [6]), Fornasier et al. (2006, [7]), Gil-Hutton et al. (2014, [8]), Manset & Bastien (2000, [9]), Ganesh et al. (1998, [10]), Chernova et al. (1993, [11], Gehrels et al. (1964, [12]).

Asteroid polarimetry is obtained in various standard filters, but more frequently in V; in case of the faint Jupiter Trojans, Centaurs, and trans-Neptunian objects, most of polarimetric measurements were obtained in the R Bessel filter, to take advantage of the fact that they appear ~ 0.5 mag brighter in this filter than in V. Polarimetry of comets is often obtained using specially designed filters covering narrow wavelength ranges that are free from gas emission lines. This way, polarization measurements are not diluted by emission lines, but represent just the polarization due to dust scattering.

2.2 Polarimetric maps

For extended objects like our Moon, comets and giant planets, it is possible to obtain polarimetric maps and correlate them with intensity and colour maps. These maps may be used to study how cometary dust changes with the distance from the nucleus, or allow one to identify (and interpret) different features of the surface or atmosphere of a planet or a comet. These data are much less commonly available than aperture polarimetry data, as they require instruments with polarimetric capabilities in a large field of view. We note that at favourable viewing conditions, the surfaces of some asteroids (e.g., Ceres, Pallas, Vesta, and Melpomene) may be resolved from ground-based measurements using the ZIMPOL polarimetric module of the new SPHERE instrument, (Beuzit et al. 2008, [19], and Thalmann et al.(2008, [20]) of the ESO Very Large Telescope (VLT). On relatively bright objects, ZIMPOL/SPHERE may reach a spatial resolution of 20 mas.

2.3 Spectropolarimetry

In the last few years, it has become evident that the way polarization depends on wavelength gives also useful constraints to the modelling of Solar System objects. For instance, compact particles may reproduce the behaviour of comet polarimetric measurements with phase-angle, but not the observed polarimetric spectral gradient (e.g. Kolokolova & Kimura 2010, [21]). Therefore, multicolour polarimetry provides evidence that cometary dust is better represented by aggregates of monomers rather than compact, even polydisperse, dust particles (Kolokolova et al. 2004, [22]). Multicolour polarimetry (Lupishko & Kiselev 1995, [23], Belskaya et al. 2009a, [24]) and spectropolarimetry (Bagnulo et al. 2015, [25]) are also promising tools for a better characterization of the surface structure of asteroids, and will be discussed later (Sect. 3.5).

2.4 Instrumentation, observing strategies, and data reduction

Some general principles of the polarimetric techniques adopted in night time astronomy, and in particular the advantage of using the so-called "beam-swapping" technique, are discussed, e.g., by Bagnulo et al. (2009, [26]). Here we add that polarimetric measurements of small bodies of the Solar System are more useful when obtained with instruments that have polarimetric capabilities in the continuum, i.e., with either very little or accurately calibrated instrumental polarization. Imaging polarimetry is useful if the entire instrument field of view is free of instrumental polarization, or at least affected by a constant (or well calibrated) instrumental offeset, and the observations are still able to reveal polarization variability across the target (e.g., a cometary coma).

In case of spectropolarimetry, low- to mid-resolution instruments such as FORS (Appenzeller et al. 1998, [27]) of the ESO VLT and ISIS of the William Herschel Telescope (WHT) are probably more useful than high-resolution spectropolarimeters such as ESPaDOnS of the Canadian-France-Hawaii Telescope (CHFT) and Narval of the Pic-du-Midi Observatory in France. The reason is that high-resolution spectropolarimeters are usually fiber-fed from a polarimetric module attached at the Cassegrain focus. The ratio between the transmission of the two channels of the polarimeter may not stay constant between an exposure and the next of a series, and this is responsible for a poor accuracy of the measurement of the polarization of the continuum. However, polarization of the spectral lines may be still measured with high-precision, and high-resolution spectropolarimetry may be useful for the study of molecular bands (e.g., LeBorgne & Crovisier 1987, [28]).

A modern and exhaustive list of facilities that may be used for polarimetric observations is given by Keller et al. (2015, [29]). Here we mention that in the latest decade, many polarimetric data have been obtained with at the Argentinian CASLEO observatory (asteroid polarimetry), with the SCORPIO-2 imaging polarimeter at the Special Astronomical Observatory in Russia and, more recently, at the 1-m Omicron telescope of the observing station of Calern (France) equipped with a new instrument built a the Torino Observatory (Italy) (Pernechele et al. 2010, [30]). Preliminary results of an asteroid polarimetric survey carried out at Calern have been published by Devogèle et al. (2017, [31]). Fainter objects such as TNOs, cometary nuclei, and Centaurs have been observed with the FORS instrument of the ESO VLT.

2.4.1 Required accuracy of the measurements

The amplitude of the observed polarimetric curves for most asteroids is usually at most $\sim 2\,\%$, therefore polarimetric measurements are useful when their uncertainties are $0.1\,\%$ or smaller. While larger errors may be tolerated when the observations are obtained at phase-angles $\geq 40^\circ$ (when the typical signals are $\geq 2\,\%$), some subtle but important differences, like those between large and small size TNOs discussed in Sect. 4.2, may be appreciated only if the measurement uncertainties are of a few units in 10^{-4} or less. Among the most accurate polarimetric measurements obtained so far are those by Wiktorowicz & Nofi (2015, [32]), who have monitored asteroid (4) Vesta during its rotational cycle, measuring a peak-to-peak variation of $\sim 3\,10^{-4}$ with typical uncertainty of $\sim 5\,10^{-5}$. Polarimetric measurements need ultra-high signal-to-noise ratio, since uncertainties are given by the inverse of the signal-to-noise (S/N) ratio. For instance a S/N ratio > 2500 is needed to obtain a polarimetric measurement with an uncertainty of $0.04\,\%$. Neglecting the contribution to the error bar from background subtraction (which we cannot do in case of faint objects), this means counting nearly 10^7 photons above background. For faint objects such as TNOs, these high S/N ratios may be obtained only with large telescopes. Note that around faint targets there are also higher chances to have a background "contaminated" by objects of brightness comparable or larger than the main target, in which case the measurement error may be substantially higher than what expected from simple photon-noise estimates. Observing strategy and data reduction techniques (including basic principles of "aperture polarimetry") are extensively discussed in Bagnulo et al. (2011, [33]) and Bagnulo et al. (2016, [34]).

2.5 Theoretical tools for physical interpretation

Depending upon the illumination conditions and the geometric albedo of the surfaces, either single scattering or multiple scattering mechanisms can play a major role in determining the resulting intensity and state of polarization of the scattered sunlight. For large phase angles, the angular dependence of polarization is mainly defined by single scattering (Fresnel's law) which is responsible for the maximum polarization located at phase angles in the range $\sim 75^\circ - 110^\circ$. However, in contrast to what follows from Fresnel's law, polarization never reaches 100 %. The reason of this is multiple scattering. Multiple scattering is accompanied by variations of the scattering plane and, thus, variations in polarization plane that reduces the total fraction of linear polarization. It is therefore not surprising that objects having higher geometric albedo, for which multiple scattering is more efficient, tend to exhibit a lower degree of linear polarization. This inverse relationship between albedo and polarization has been observed numerous times for a variety of objects and is known as the *Umov law* (Umov 1905, [35]).

Multiple scattering plays a completely different role at small phase-angles, where it is the main mechanism responsible for the negative polarization. After moderately successful attempts in the 80s to explain negative polarization in the framework of multiple Fresnel reflections (Wolff 1980, [36], Wolff 1981, [37], Kolokolova 1990, [38]), a major step forward has been the recognition of the role played by the so-called Coherent Backscattering Mechanism (Shkuratov et al. 1994, [39], Muinonen 1994, [40]). Its physics is constructive interference of the multiply scattered light that traveled through the medium along identical optical paths but in opposite directions – the situation geometrically most common for the backscattered light. This mechanism is considered to be essential to understand both the phenomenon of brightness opposition effect (a non linear increase of brightness occurring close to solar opposition, see Sect. 3.2), as well as the presence of a negative polarization branch. The modelling efforts are steadily progressing these days, through analytical and experimental analyses of the light scattering properties of assemblages of particles thought to be suited to represent the behaviour of the surface regolith of asteroids and other classes of Solar System bodies (Muinonen et al. 2015, [41]).

To the contrary of the light scattering by regolith surfaces, the scattering by cometary dust does not invoke multiple scattering between particles and the phase dependence of cometary polarization can be reproduced even by an ensemble of polydisperse spherical particles (Mukai et al. 1987, [14]). However, scattering by such an ensemble cannot reproduce other photopolarimetric characteristics of cometary dust, e.g. its photometric color and spectral gradient of polarization. It also fails to explain observations of cometary dust in thermal infrared (Kolokolova et al. 2004, [22]). Currently, the majority of the models of cometary dust is based on aggregated/agglomerated model, i.e. when a single dust particle consists of a number of small grains called monomers. Computations of the light scattering by such particles is usually based on two main light-scattering techniques: T-matrix approach by Mackowski & Mishchenko (1996, [42]) and Discrete Dipole Approximation (DDA) by Draine & Flatau (1994, [43]) and their variations. T-matrix code considers cometary particles as clusters of spheres, which can consist of thousands of monomers (Kolokolova & Mackowski 2012, [44]). DDA is capable to build particles with grains of a variety of shapes, although, due to computer limitations, is now limited by particles of radius $\leq 4\,\mu$m (Zubko et al. 2014, [45]). One of the advantages of the aggregated model of cometary dust is that it is consistent with the current ideas of comet formation in the protoplanetary nebula and with the studies of interplanetary dust particles (IDPs) of cometary origin and samples of the dust in comet Wild 2 returned by Stardust mission.

3 Main-belt asteroids

Main-belt asteroids are the most popular targets among Solar System objects, for the simple reason that they are numerous and relatively bright. Polarimetric observations of asteroids can be used to get information on albedo, size and surface regolith texture. For a long time, this has been the subject of an eminently empirical approach, based on the results of laboratory experiments. Early investigations were based on measurements of the polarimetric properties of the light scattered by specimens of terrestrial minerals, lunar fines and crushed meteorites. The main results of these investigations were published in the 70s in a series of classic papers (see review by Dollfus & Zellner 1979, [46], and references therein) in which the foundations of modern asteroid polarimetry were laid.

Figure 3 shows the polarization curves of the first four asteroids discovered in the XIX century. The morphology of the polarization curves of these objects, that belong to different taxonomic classes and are characterized by low (Ceres and Pallas), intermediate (Juno) and medium-high (Vesta) albedo, is similar in its general trend. It can be adequately represented by Eqs. (4) or (5).

3.1 Asteroid geometric albedos from polarimetry

The *geometric albedo* is the ratio between the body brightness at zero-phase angle (perfect opposition) and the brightness of a perfectly diffusing disk in the same position and with the same apparent size of the body. The *absolute*

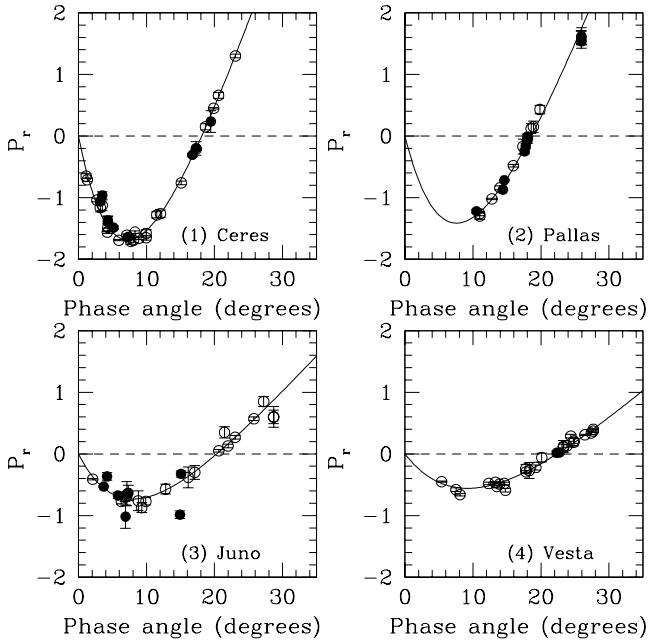

Fig. 3. Examples of phase - polarization curves obtained for four large main belt asteroids belonging to different taxonomic classes. Sorting by increasing albedo, top left: the dwarf planet (1) Ceres (G-class); top right: (2) Pallas (B-class); Bottom left: (3) Juno (S-class); bottom right: (4) Vesta (V class). Open symbols refer to data available in the literature in the V filter. Full symbols in the plots identify observations obtained at the CASLEO observatory (San Juan, Argentina, most of which published by Gil-Hutton et al. 2014, [8]). Solid lines are the best-fits obtained via Eq. (5). We note that the lower the albedo, the deeper the polarisation minimum, and the steeper the curve around the inversion angle. We also note that (2) Pallas is an example of an object having a relatively high orbital inclination, which is difficult to observe at small phase angles.

magnitude of an asteroid is the apparent magnitude that would be measured by observing the object at zero phase-angle and at unit distance from both the Sun and the observer. In most of the cases, the absolute magnitude is referred to the V filter.

Geometric albedo and absolute magnitude are linked to the asteroid size through the relationship

$$\log(D) = 3.1236 - 0.2\,H - 0.5\log(p_V) \tag{6}$$

where D is the diameter expressed in km (assuming that the object is spherical), p_V is the geometric albedo, and H is the absolute magnitude, both measured in the V filter. Equation (6) may be used to determine the asteroid diameter if the absolute magnitude and the geometrical albedo are known, or to determine the albedo if the absolute magnitude and diameter are known. The absolute magnitude of the asteroid is extrapolated from photometric measurements taken at different phase angles, and in many cases its uncertainty is actually non-negligible.

The so-called thermal radiometry technique, which measures the flux at mid-IR wavelengths, is particularly suitable to infer asteroid sizes (Masiero et al. 2011, [47]). This is due to the fact that the thermal flux of asteroids strongly depends on the size of the emitting body. Added to an estimate of the absolute magnitude, thermal radiometry is commonly used to derive asteroid albedos. However, the accuracy of this method is usually rather low, due both to the uncertainty of the thermal models and to the limited accuracy of the estimates of the absolute magnitude (Cellino et al. 2015a, [18]).

In fact, polarimetry may be used to estimate the asteroid geometric albedos. This is due to the existence of relations between geometric albedo and polarimetric properties resulting from the Umov law discussed in Sect. 2.5, that have been known since the time of the first laboratory experiments (see Cellino et al. 2015b, [48], and references therein).

Figure 3 shows polarimetric curves with different slopes and minima. Curves with deeper minima have steeper slopes at the inversion point, and, *vice versa*, when the minimum is shallower, also the slope is less steep. This reflects the fact that the albedo of these asteroids are quite different. Objects such as Ceres and Pallas, that have reflectance spectra similar to those of low-albedo, carbonaceous chondrites, are characterized by deeper negative polarization values and steeper values of the h polarization slope. An opposite trend is displayed by objects, like Juno and Vesta, characterised by reflectance spectra similar to those of meteorites with increasingly higher albedo, namely ordinary chondrites (Juno) and HED achondrites (Vesta).

The possibility to estimate the albedo through polarimetric measurements is a quite remarkable opportunity, because photometry alone cannot distinguish an object bright and small from one large and dark. The combination of polarimetry and photometry is one of the techniques that allows us to estimate the asteroid size (through Eq. (6). Obviously, the accuracy of the estimates of the absolute magnitude represents a limiting factor in the estimate of the asteroid size also when the albedo is estimated via polarimetric techniques.

The empirical relationships between albedo and minimum of the polarization and slope have been generally expressed as

$$\begin{aligned} \log_{10}(p) &= C_1 \log_{10}(h) + C_2 \\ \log_{10}(p) &= C_3 \log_{10}(P_{\min}) + C_4 \end{aligned} \tag{7}$$

where the values of coefficients C_i vary between ~ -1.8 and ~ -0.8. The exact values of these coefficients depend on certain choices made to calibrate these relationships. Zellner et al. (1977, [49]; see Cellino et al. 2015a, [18]) have also pointed out the existence of a degeneration of the slope - and $P_{\min}$ – albedo relationships for small albedo values.

A "historical" problem in asteroid polarimetry was to obtain an accurate calibration of these relationships, i.e., finding accurate values for the C_i coefficients. A list of asteroids that are ideally suitable to be used for these purposes was published by Shevchenko and Tedesco (2006, [50]). This list includes 61 asteroids with accurate estimates of the absolute magnitude, and extremely accurate measurements of the size, obtained by either *in situ* measurements by space probes, or by observations of stellar occultations. Combining these data with polarimetric measurements (many of which acquired during the dedicated observing campaigns at the CASLEO observatory in Argentina), Cellino et al. (2015a, [18]) have obtained updated estimates for these coefficients, and suggested for instance

$$\begin{aligned} C_1 &= -1.111 \pm 0.031 \qquad C_2 = -1.781 \pm 0.025 \\ C_3 &= -1.419 \pm 0.034 \qquad C_4 = -0.918 \pm 0.006 \, . \end{aligned}$$

In fact, Cellino et al. (2015a, [18]) have proposed *various* sets of calibration coefficients that may be best suitable in certain specific cases, including for instance one set of parameters derived by excluding calibration asteroids with albedo < 0.08. They also suggested the use of a new polarimetric parameter, $\Psi = P_{\rm r}(\alpha = 30^\circ) - P_{\rm r}(\alpha = 10^\circ)$, where the $P_{\rm r}$ values are taken from the best-fit of the phase – polarization curve obtained via Eq. (5). According to Cellino et al. (2015, [18]), the use of this new Ψ parameter leads to accurate albedo estimates both for bright and dark asteroids.

3.2 Opposition effects

A phenomenon that is often observed is the so-called brightness opposition effect, namely a non-linear brightness surge occurring when an asteroid is observed at very small phase-angles (a few degrees), when approaching solar opposition. The opposition effect is a complicated phenomenon, because it varies much among different asteroids, being nearly absent in some cases, and quite strong in other cases.

A polarimetric version of the opposition effect, consisting of a negative polarization peak at phase-angles $\leq 2^\circ$, has been observed so far in the case of a couple of very-high albedo asteroids, (44) Nysa and (64) Angelina, belonging to the E taxonomic class (Rosenbush et al. 2005, [51], Rosenbush et al. 2009, [52]), and in three Jupiter satellites (see Sect. 5.2). However, this effect is very small compare to the typical error bars, hence there is not a general consensus that this phenomenon is real and shared by a larger number of objects. Nevertheless, if real, the polarization opposition effect should be regarded as an important constraint for theoretical models of light scattering processes.

3.3 The contribution of polarimetry to asteroid taxonomy

When we obtain spectroscopy of asteroids, we basically measure the reflected spectrum of the sun. In fact, hidden in the solar spectrum, asteroids display some spectral features, that may be revelead by dividing the target spectrum by the spectrum of a solar analogue star (i.e., a star of same spectral type as the sun) obtained with the same instrument and instrument setting. The result of this division is the so-called "reflectance spectrum" of the asteroid. In the same way as stars are classified in various spectral types based on their spectra, asteroids can be grouped in different taxonomic classes based on their reflectance spectra. There are some differences, though. Stars are classified mainly based on the spectral lines that are formed in their atmospheres, and stellar spectra can be often straightforwardly interpreted in terms of atmospheric chemical composition, temperature and gravity. Compared to most of stellar spectra, asteroids reflectance spectra do not have narrow-band features; their main distinctive characteristics are their slope and the frequent presence of broad absorption bands, which may disclose the nature of the surface through a comparison with mateorite spectra studied in the laboratory. This is not a trivial task, though. The proposed interpretations are often non unique, and there is always some risk, when comparing the spectroscopic properties of meteorites with those of natural celestial bodies in their natural environment and with their own properties of soil texture and micro-roughness.

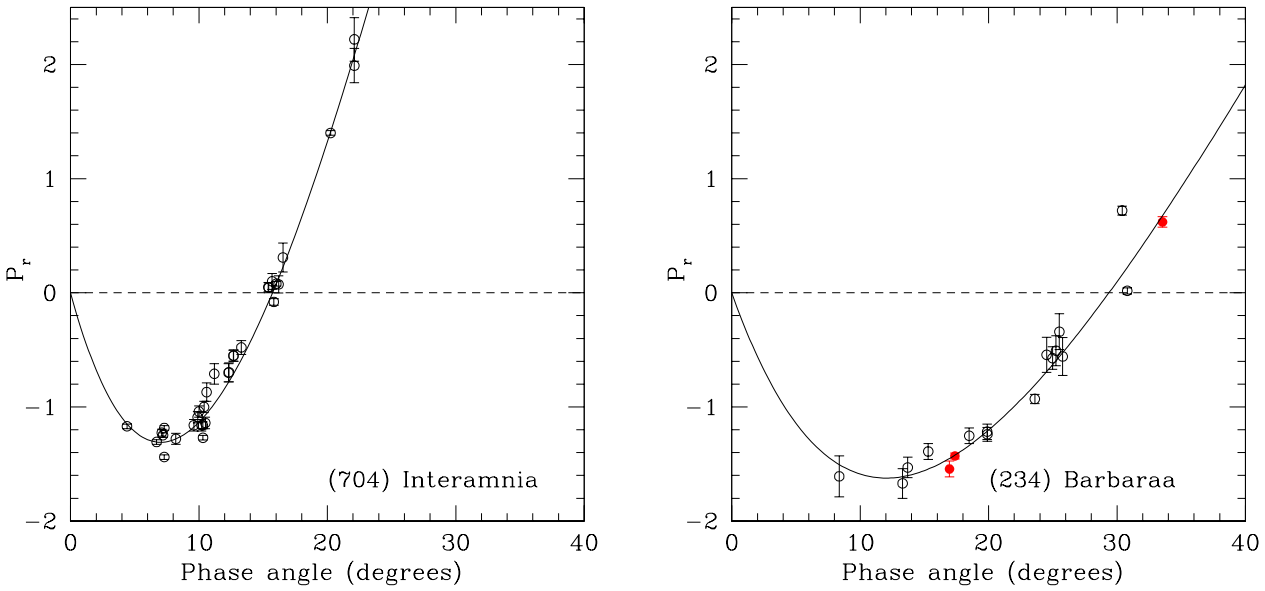

Fig. 4. Phase–polarization curve in the V filter of asteroids (704) Interamnia, the biggest asteroid belonging to the F class (left panel) and of (234) Barbara, the prototype of Barbarian asteroids (right panel). The inversion angles are $\sim 16^\circ$ for Interamnia and $\sim 29.5^\circ$ for Barbara.

Modern taxonomic classifications of asteroids are based upon analysis of visible and near-IR reflectance spectra (Bus & Binzel 2002, [53]; DeMeo et al. 2009, [54]). Polarimetry may also be used for taxonomic classification purposes. In fact, the geometric albedo derived from polarimetry is an important parameter for taxonomic classification, and it was used in the past to distinguish among objects that exhibit nearly identical spectral reflectance data at visible wavelengths, but strongly differ in terms of albedo, implying completely different surface compositions and thermal histories. Moreover, according to Penttilä et al. (2015, [16]), Eq. (4) can be used to parametrise the phase - polarization curves and develop an asteroid taxonomic classification nicely consistent with those traditionally obtained by means of spectroscopy. It was also shown that multicolour polarimetric data allows one to refine asteroid taxonomy (Belskaya et al. 2017, [55]). However, polarimetry should not be seen as a parallel system for asteroid classification, in fact, polarimetry would not be particularly useful if it was bringing the same information as intensity spectra; in the remaning part of this Section we will elaborate this concept, and discuss a few examples which show how polarimetry may complement spectroscopy for asteroid taxonomic classification.

3.3.1 F-type asteroids

In the spectroscopic classifications published in the 80s, there were two rather rare sub-classes of primitive asteroids, that were named B and F (the latter having been first defined by Gradie & Tedesco 1982, [56]), which could be distinguished from their spectra slope at short wavelengths – the F class being characterized by a quite flat trend. Asteroids originally belonging to these two classes were later merged into a unique B class in the most recent classification by Bus & Binzel (2002, [53]). Yet, polarimetry tells us that the old F class is clearly separated from the B and all other asteroid classes, due to the property of having unusually low values of the inversion angle (Belskaya et al. 2005, [57]). An example of this behaviour is given by the phase - polarization curve of asteroid (704) Interamnia shown in the left panel of Fig. 4.

The F class is very interesting in many respects. For instance, an F class asteroid, (3200) Phaeton, is known to be the source of the Gemini meteors, while comet 107P/Wilson Harrington was first discovered as an asteroid (numbered 4015), classified as CF by Chamberlin et al. (1996, [58], and references therein.) These facts suggest the possibility that F-class asteroids exhibit cometary properties. This inference is strengthened by the fact that Boehnhardt et al. (2008, [59]) and Stinson et al. (2016, [60]) found that a few cometary nuclei observed at heliocentric distances at which no coma was visible, exhibit the same polarimetric properties as F-class asteroids (namely a low value of the inversion

angle), and by the fact that 133P/Elst-Pizarro – a main-belt object that shows cometary activity – has polarimetric characteristics similar to those of F-type asteroids (Bagnulo et al. 2010, [61]).

3.3.2 The Barbarians: very primitive remnants of the early Solar System?

Cellino et al. (2006, [62]) discovered that asteroid (234) Barbara had a polarimetric curve characterized by an unusually large inversion angle, $\sim 30^\circ$ (see right panel of Fig. 4).

New polarimetric observations by Gil-Hutton et al. (2008, [63]) and Masiero & Cellino (2009, [64]) brought the total number of known Barbarians to about half a dozen, including objects belonging to the L, L_d and K taxonomic classes of Bus & Binzel 2002, [53]). More recently it has been realized that the all known Barbarians belong to the new L-class of the taxonomic classification by DeMeo et al. (2009, [54]), which is based on an extension of spectral reflectance data to the near-IR region.

At the same time, it was discovered that most known Barbarians, e.g., particular (234) Barbara, (387) Aquitania, and (980) Anacostia, exhibit very unusual reflectance spectra, characterized by anomalously high abundance of the spinel mineral (Sunshine et al. 2008, [65]). Spinel is a refractory mineral thought to be among the most ancient samples of solid material found in our Solar System. It is common in Calcium-Aluminum-rich inclusions (CAI) found in carbonaceous chondrite meteorites. CAIs are possibly the oldest samples of solid material found in our planetary system. In the case of Barbarian asteroids, the big difference is that the abundance of spinel on their surfaces, as inferred from analyses of the reflectance spectra, is thought to be three times the maximum abundances of the same mineral found in CAIs (Sunshine et al. 2008, [65]). We know therefore that Barbarians are possibly extremely primitive, but their history is not clear.

More recently, Cellino et al. (2014, [66]) discovered that one dynamical family, named after asteroid (729) Watsonia, is mostly composed of small Barbarians. Moreover, two of the biggest Barbarian and spinel-rich asteroids, namely (387) Aquitania and (980) Anacostia are close to each other, and to the Watsonia family in the space of orbital proper elements, although not sufficiently close to be recognized as members of a same dynamical family.

Tentatively, we may sketch the following scenario: Watsonia family members could be the outcome of a second-generation impact that in relatively recent times destroyed a Barbarian parent body, which in turn was one of the first-generation fragments of a much larger original parent body destroyed a very long time ago. This original family is no longer identified because all the small members of it have long been removed by collisions and Yarkovsky-driven dynamical evolution (Bottke et al. 2002, [67]). Only the biggest fragments of the first generation, including (387) Aquitania, (980) Anacostia and the parent body of the more recent Watsonia family were left in their original location in the orbital elements space. They had sufficient time to experience a very gentle dynamical dispersal that makes them no longer recognizable as members of the same family. The fact that these Barbarians are all spinel-rich and may be therefore extremely primitive suggests that they might well be among the very few remnants of an early population of planetesimals originally formed in this region, or brought there early during the first chaotic phases of evolution of the planetary system, possibly before the epoch of the so-called Late Heavy Bombardment (Wetherill 1975, [68]). Because it is known that 99 % of the original population of planetesimals accreted in the region of the current asteroid belt was removed in the early phases of Solar System's history, this might explain why Barbarians are so rare. Of course, this kind of interpretation is only essentially a conjecture at this stage, and new observational evidence and theoretical modelling are necessary before drawing any conclusion. However, this conjecture still represents an interesting example of how polarimetric measurements may help us to reconstruct the evolution of the Solar System.

3.3.3 Physical characterization of Near Earth Asteroids

Several asteroids, including low-albedo, primitive ones, are currently present in the inner solar system in the region of the terrestrial planets. These are the objects collectively called Near-Earth Asteroids (NEAs). Low-albedo NEAs are currently considered by the scientific community as very important potential targets for future space missions aimed at returning to Earth samples of pristine material from the epoch of planetary growth. In many cases, NEAs may be observable at very large phase angles, up to $100 - 120^\circ$. In these conditions, even one single polarimetric measurement, obtained at phase angle larger than 40°, may allow us to discriminate between low, medium or high albedo. At present, however, only less than 10 NEAs have been observed using polarimetry (De Luise et al. 2007, [69], Belskaya et al. 2009b, [70], Belskaya et al. 2015, [71], Fornasier et al. 2015, [72]; see also Lupishko 2014 [73]), mostly due to the faintness of the objects.

3.4 Other constraints from polarimetry

Beside albedo determination and taxonomic classification, polarimetric observations may bring a variety of additional constraints.

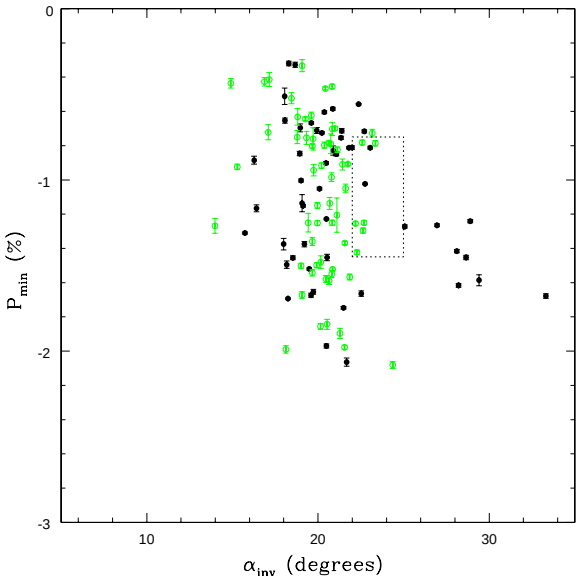

Fig. 5. Inversion angle - $P_{\rm min}$ plot for all asteroids for which the phase - polarization curve is sufficiently well characterised that can be fit by using Eq. (5). Some data points are based on still unpublished observations recently obtained in the framework of the Calern Asteroid Polarimetric Survey (Devogèle et al., 2017, [31]). Full black symbols correspond to asteroids for which we have at least 10 observations; open green symbols refer to asteroids with a number of observations between 5 and 9. The small rectangular domain in the middle-right part of the plot corresponds to the domain of thin lunar fines that was shown in some classical plots published by Dollfus et al. (1989, [74]).

An example is given by an analysis of the relation between polarimetric parameters including the inversion angle $\alpha_{\rm inv}$ and the extreme value of negative polarization $P_{\rm min}$. Figure 5 shows a modern reassessment of a classical plot $\alpha_{\rm inv} - P_{\rm min}$ already analyzed some decades ago by Dollfus et al. (1989, [74]), who showed that the asteroid data available at that time occupied in this plot a domain between two major regions: one at lower values of $\alpha_{\rm inv}$, corresponding to polarimetric properties of bare chips or large fragments of rocks analyzed in the laboratory), and one at higher values of $\alpha_{\rm inv}$, corresponding to the behaviour exhibited by very thin powders of lunar material. In the $\alpha_{\rm inv} - P_{\rm min}$ diagram, the asteroid domain is shared with the one obtained from laboratory measurements of pulverized rocks with particle sizes between 30 and 300 μm. Dollfus et al. (1989, [74]) demonstrated the use of polarimetric data as a remote diagnostic tool to derive information on the texture and general properties of surface regolith covering atmosphereless Solar System bodies, and proposed an explanation of the data based on the idea that meteoroid collisions on the Moon progressively pulverize down to very small sizes the surface regolith particles, with negligible loss of material due to the strong gravitation of the Moon. In the case of asteroids, Dollfus et al. (1989, [74]) suggested that the much weaker gravitation of these objects allowed most of the smallest and fastest ejecta produced in collisions to escape to infinity, leaving behind a much coarser regolith with respect to that of the Moon. This interpretation cannot be ruled out even today, but the situation is now more complex, as the inventory of asteroid polarimetric data has largely increased. A major difference is due to the presence of some asteroids which are found much closer to or within the domain of strongly pulverized material. Known Barbarian asteroids, including (234) Barbara, (172) Baucis, (387) Aquitania and (980) Anacostia, and (236) Honoria, all of them having $\alpha_{\rm inv} > 26^\circ$, are located even beyond the high-$\alpha_{\rm inv}$ end of the domain of fine powders considered by Dollfus et al. (1989, [74]). In addition, one non-Barbarian asteroid, (21) Lutetia, a large object ($D > 100$ km), visited in 2010 by the Rosetta spacecraft (Sierks et al. 2011, [75], has $\alpha_{\rm inv} \sim 25^\circ$ and $P_{\rm min} \sim -1.27\,\%$ (Belskaya et al. 2010b, [76]; 2017, [55]), which put this asteroid within or very close to the high-$\alpha_{\rm inv}$ end of the domain of finely pulverized rocks and lunar fines. The Rosetta fly-by of Lutetia revealed a heavily cratered, and possibly non-convex, shape (Farnham 2013, [77]). In this respect, it is interesting to note that Keihm et al. (2012, [78]) carried out an extensive analysis of Rosetta thermal flux data of Lutetia and concluded that this asteroid has a quite low thermal inertia, suggesting that its surface is probably rich in fine dust (see also Lamy et al. 2010, [79] and Coradini et al. 2011, [80]).

The possible presence of large concavities seems also to be associated with a polarimetric behaviour characterized by a large value of the inversion angle (there is evidence that (234) Barbara is quite a elongated object with large concavities, see Cellino et al. 2006, [62] and Tanga et al. 2015, [81]). This is a subject that deserves further investigations.

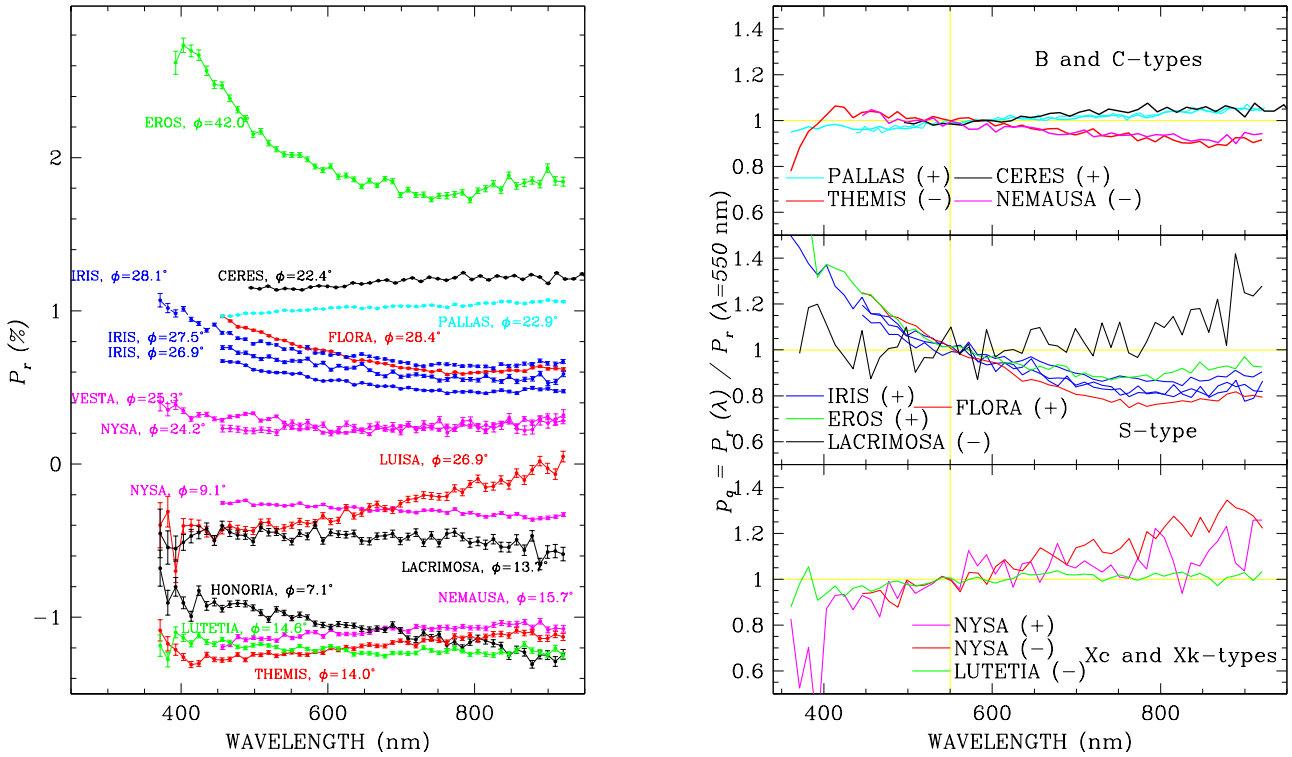

Fig. 6. Left panel: polarization spectra of asteroids observed at different phase-angle. Right panel, normalised polarization spectra for a target sub-sample. The + and − symbols indicate whether the object has been observed in the positive or negative branch of polarization, respectively.

3.5 Spectropolarimetry

A further subject of investigation is how polarization depends on wavelength, and if polarization spectra may be used for a more refined classification of the asteroid.

The left panel of Fig. 6 shows the polarization spectra of various asteroids of different taxonomic classes, obtained at different phase angles (Bagnulo et al. 2015, [25]). Their comparison is not straightforward, even when spectra appear totally different (like, e.g., in the case of Pallas and Eros). In principle, the observed differences might due either to the fact that the spectra were obtained at different phase-angles, or to differences in the surface structure of the asteroids, or both. Bagnulo et al. (2015, [25]) have therefore introduced a new quantity, i.e., the polarization spectrum normalized to the value at a certain arbitrary wavelength, e.g. 550 nm. Under the hypothesis that at least at first order the polarization spectra may be expressed as the product of two functions, one that depends only on phase-angle, and one that depends only on wavelength, $P_{\rm r}(\lambda,\alpha) = p'(\lambda)\,A(\alpha)$, then the normalised polarization spectrum

$$p(\lambda) = \frac{P_{\rm r}(\lambda,\alpha)}{P_{\rm r}(\lambda = 550\,{\rm nm},\alpha)} = \frac{p'(\lambda)\ A(\alpha)}{p'(\lambda = 550\,{\rm nm})\ A(\alpha)} \tag{8}$$

is independent of the phase-angle. Practically, it is necessary to associate to each asteroid at least two polarization spectra, one for the negative branch, and one for the positive branch. The right panels of Fig. 6 show the $p(\lambda)$ spectra of a sub-set of the asteroids of the left panel of the same Figure.

In agreement with previous results obtained with multicolour polarimetry by Lupishko & Kiselev (1995, [23]) and Belskaya et al. (2009a, [24]), Bagnulo et al. (2015, [25]) have shown that P_Q spectra of low-albedo asteroids have a positive gradient, and P_Q spectra of intermediate-albedo asteroids always have a negative gradient. We note that this means that the *absolute value* of the polarization of low-albedo asteroids has a negative gradient in the negative branch and a positive gradient in the positive branch. Vice versa, the absolute value of the polarization of intermediate-albedo asteroids has a positive gradient in the negative branch and a negative gradient in the positive branch.

In Sect. 2.5 we mentioned that in the case of high-albedo bodies, multiple scattering can reach higher orders of scattering and, thus, the depolarization of light by multiple scattering is stronger for higher albedo than for lower albedo surfaces. Therefore, we expect that if the reflectance spectrum of an asteroid increases with wavelength, then

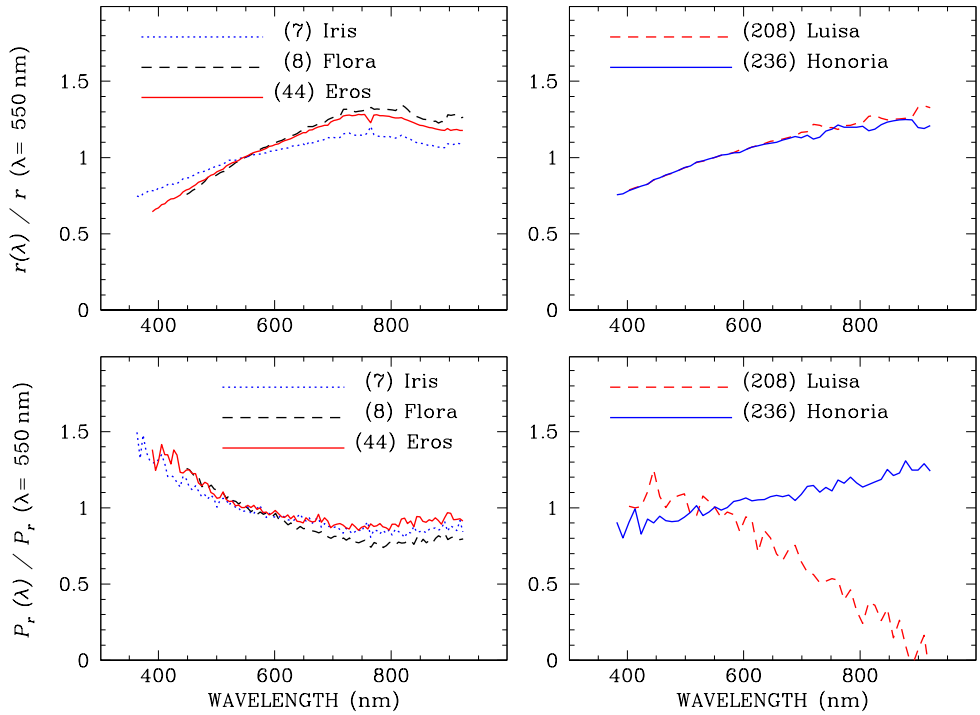

Fig. 7. Top panels: reflectance spectra for five asterods; right panels: the normalised polarization spectra of the same five asteoroids. The left panels show spectra obtained in the positive branch, and all of them obey the Umov law. The right panels show spectra obtained in the negative branch, and in case of asteroid (236) Honoria, the Umov law is violated. Data taken from Bagnulo et al. (2015, [25]).

the absolute value of the polarization decreases with wavelength, and viceversa. This behaviour is seen in many cases (e.g., in S-type asteroids, see top panels of Fig. 7), and is the Umov effect mentioned in Sect. 2.5. However, Umov effect does not appear ubiquitous in asteroid polarization spectra. The bottom panels of Fig. 7 shows the reflectance and polarization spectra of asteroid (236) Honoria and (208) Luisa, that were observed in the negative branch. The reflectance spectra of these two asteroids appear very similar, but the wavelength gradients of their polarization spectra have opposite sign, and in particular, data of (236) Honoria show that Umov law is violated. An explanation can be given by considering that the polarization behaviour in the negative branch is the result of the relative contribution of three competing mechanisms: (1) polarizing effect of coherent backscattering; (2) depolarizing effect of non-coherent multiple scattering, and (3) shadow hiding. Shadow hiding does not depend on albedo, so the main competitors are coherent backscattering and non-coherent multiple scattering. Coherent backscattering is more efficient for high albedo objects because, due to a higher efficiency of multiple scattering in such objects, there are more opportunities for light to be scattered under the conditions that result in the constructive interference. Non-coherent scattering is also more efficient for high albedo objects where multiple scattering can reach higher orders before the light is absorbed; this results in a higher depolarized component in the scattered light. Which mechanism dominates, strongly depends on the size of regolith particles and their packing. In the situations when non-coherent backscattering dominates, depolarization increases, and, thus, the absolute value of polarization decreases with albedo. When coherent backscattering dominates, the light reflected by higher albedo surfaces is more polarized than the light reflected by lower albedo surfaces. This apparent complex situation actually shows how spectropolarimetric measurements may be used as a remote sensing tool to estimate physical characteristics of the regolith, and at the same time demonstrates the need of increasing the currently available data-set to improve our understanding and base our interpretation attempts on a more robust body of evidence.

We finally comment that in asteroid spectroscopy, the choice of the solar analogue used for the normalisation of the intensity spectra and the quality of the calibration of the atmospheric extinction may sometimes affect the reflectance spectra, and, ultimately, the taxonomic classification of asteroids. By contrast, spectropolarimetric measurements are independent of atmospheric conditions, and do not require any calibration with a solar analogue star. If the instrumental polarization is low and under control, they may be perfectly reproduced even with different instruments.

However, spectropolarimetric techniques still allow us to obtain simultaneously also reflectance spectra, provided that the usual calibrations are performed, therefore they can nicely complement traditional spectrophotometric techniques.

4 Jupiter Trojans, Centaurs, and Kuiper-Belt objects

With the exception of Pluto (Kelsey & Fix 1973, [82], Breger & Cochran 1982, [4], Avramchuk et al. 1992, [83]) and the Jupiter Trojan (2797) Teucer (Fornasier et al. 2006, [7]), all polarimetric investigations of Jupiter Trojans asteroids, Centaurs and Kuiper-belt objects published so far have been carried out with the FORS1/2 instrument of the 8 m VLT.

4.1 Jupiter Trojans

Trojan asteroids are confined by solar and planetary gravity to orbit the Sun 60° ahead (L4 Lagrange point of the binary system planet-Sun), or behind (L5 Lagrange point) a planets position along its orbit. Because of their dynamical stability, they allow us to look at the earliest stages of the formation of our Solar System (for a recent review on Jupiter Trojans see Emery et al. 2015, [84]). Bagnulo et al. (2016, [34]) have performed a pilot study of the polarization properties of Jupiter Trojan asteroids, and obtained measurements for six objects belonging to the L4 population. These objects exhibit similar but not identical polarization properties. Considering all objects together, $P_{\rm min}$ is reached at phase-angle $\sim 10°$, and is in the range from $-1.3\,\%$ to $-1.0\,\%$. This behaviour is very similar to that displayed by low-albedo main-belt asteroids (C, D and P classes), and is quite different from that of some Centaurs, which are found to reach $P_{\rm min}$ at much smaller phase-angles.

4.2 Centaurs and TNOs

The investigation of the physical properties of Centaurs and TNOs is more difficult than those of main-belt asteroids. Because of their distance, these objects are faint (typically $R > 18$) and, except for simple multi-colour photometry, they require the use of large telescopes. Polarimetric studies suffer also from the fact that the observable phase-angle range is extremely limited: $\lesssim 7°$ for Centaurs, and $\lesssim 2°$ for TNOs. Nevertheless, the pioneering study by Boehnhardt et al. (2004, [3]) of the polarization properties of the TNO Ixion, observed in the limited phase-range $[0°, 2°]$, revealed a quite interesting and unexpected result, namely a polarimetric curve much steeper than anything else observed before, reaching the value $-1\,\%$ already at $\alpha = 1°$.

Currently, polarimetric measurements are available for 13 TNOs and Centaurs (see Bagnulo et al. 2008, [1], Belskaya et al. 2010a, [85], Belskaya et al. 2012 [86], and references therein). In addition, there exist polarimetric measurements of the Pluto-Charon system obtained between 1972 and 1988 by several authors (Kelsey & Fix 1973, [82], Breger & Cochran 1982, [4], Avramchuk et al. 1992, [83]). Bagnulo et al. (2008, [1]) found that largest and smaller size TNOs have distinct polarimetric properties (see Fig. 8); Bagnulo et al. (2008, [1]) noted that the larger objects have a higher albedo than the smaller ones, and have the capability of retaining volatiles such as CO, N2 and CH4, and suggested that both facts may be inked to their different polarimetric behaviour compared to smaller objects. Later, Belskaya et al. (2010a, [85]) found that the polarization behaviors of the Centaurs are different from each other and from TNOs (see Fig. 8).

The most detailed polarization phase dependence covered the phase-angle range from 0.5° to 4.2° was obtained for the Centaur Chiron (Bagnulo et al. 2008, [1], Belskaya et al. 2010a, [85]), which shows a pronounced branch of negative polarization with a minimum of about $-1.4\,\%$ occurring at phase-angle as small as 1.5°. This is among the smallest values of the phase-angle of $P_{\rm min}$ as compared to any other Solar System object observed so far (similar features are shown by icy satellites of Jupiter and Uranus, see Rosenbush et al. 2015, [89]). The phase curve of Chiron is highly asymmetric, with a predicted inversion angle of $7° - 9°$ (Belskaya et al. 2010a, [85]). Polarimetric measurements of three other Centaurs, Chariklo, Pholus, and (29981) 1999 TD10 (see Belskaya et al. 2010a, [85], and references therein) revealed a great diversity in polarization properties with the negative polarization varying from $-1\,\%$ to $-2\,\%$.

The resonant TNOs Huya and Ixion also show a deep negative branch of polarization at small phase-angles, which for Huya reaches $-1.6\,\%$ at $\alpha \sim 2°$. Similar polarization phase behavior was measured for two other TNOs, the resonant object (26375) 1999 DE9, and the member of the classical population (20000) Varuna (Bagnulo et al. 2008, [1]). All these TNOs show very similar polarization phase-angle behaviors within the errors with a rapid increase (in absolute terms) of the negative polarization in the measured phase-angle range from near zero to $1° - 2°$. The polarization-phase dependence of the large classical object (50000) Quaoar displays a different behaviour compared to Centaurs and smaller size TNOs. Its negative polarization branch is shallower, and changes slowly with the phase-angle (Bagnulo et al. 2006, [87]). Very slow changes of polarization with phase-angle were also found for the largest

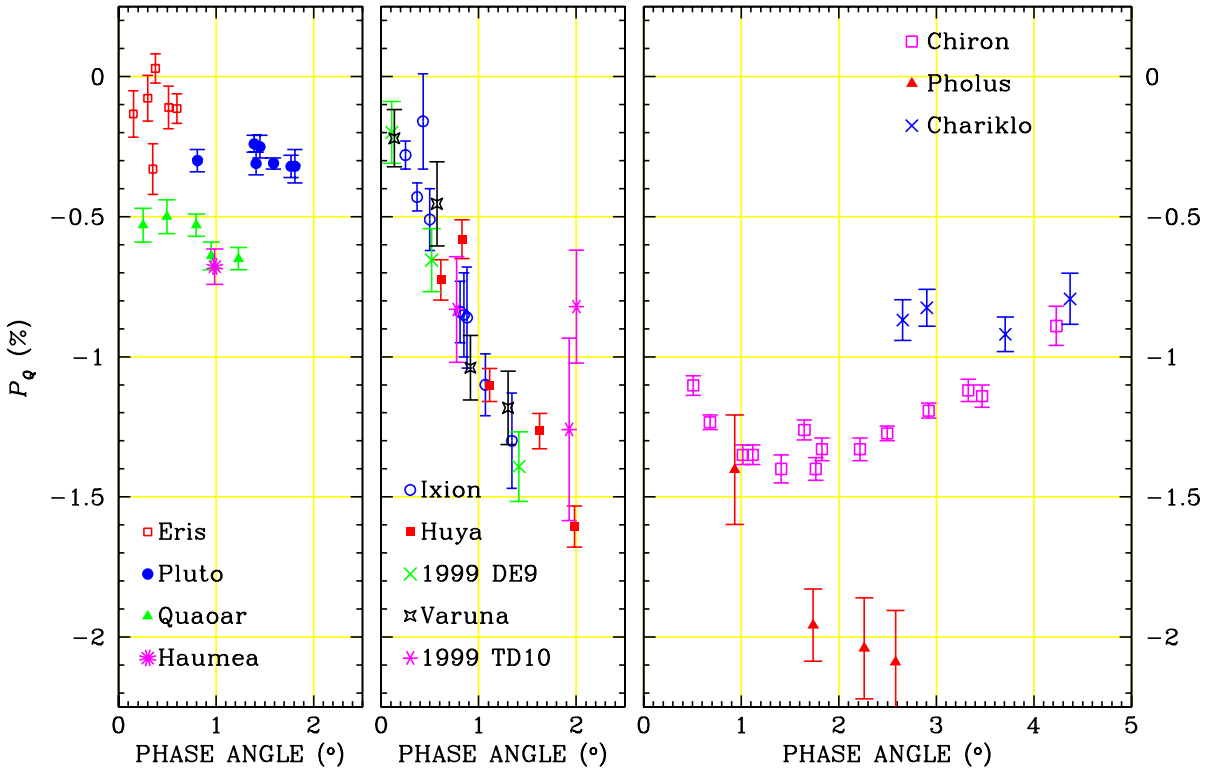

Fig. 8. Polarimetric curves for large and small TNOs (left and mid panel, respectively), and for Centaurs (rightmost panel). Data from Boehnhardt et al. (2004, [3]), Bagnulo et al. (2006, [87]), Bagnulo et al. (2008, [1]), Belskaya et al. (2008a, [88]), Belskaya et al. (2010a, [85]).

transneptunian objects Eris, Pluto, and Makemake (Kelsey & Fix 1973, [82], Belskaya et al. 2008a, [88], Belskaya et al. 2012, [86]).

Numerical modeling of coherent-backscattering shows that a possible way to explain the polarization properties of TNOs is to assume two-component surface media consisting of Rayleigh scatterers with small and large single-scattering albedos. Examples of model fits are given by Boehnhardt et al. (2004, [3]), Rousselot et al. 2005, [90]), and Bagnulo et al. (2006, [87]). Laboratory polarimetric measurements of particulate surfaces support this conclusion: mixtures of powders of different geometric albedos noticeably increase the negative polarization as compared to that of the individual mixture components. An addition of large portion of submicron-sized particles leads to asymmetric negative polarization branches with the polarization minima shifting toward small phase-angles (see Shkuratov et al. 2002, [91]). Dougherty & Geake (1994, [92]) measured the deep negative polarization branches at small phase-angles for a very thin frost layer of submicron ice crystals on the top of a dark surface. Their polarization-phase behaviours are very similar to that found for Centaurs and small TNOs. Thus, the measured diversity in polarization-phase dependences of TNOs and Centaurs can be naturally explained by different abundance of ices on their surfaces. Polarimetric properties may depend not only on ice abundance but also on ice composition, as the methane-ice rich and water-ice rich large TNOs display distinctly different polarization properties: the methane-rich TNOs Eris, Pluto, and Makemake show similar very shallow phase-angle dependences with the depths of polarization $\simeq -0.3\,\%$ (Belskaya et al. 2012, [86]), while the negative polarization branches of water-ice rich bodies is far deeper. Two water-ice rich objects of different sizes and albedos, Haumea and Quaoar, measured at the same phase-angle $\alpha \sim 1°$, show practically identical polarization $\simeq -0.7\,\%$ (Bagnulo et al. 2006, [87]; Bagnulo et al. 2008, [1]). In any case, polarimetric measurements suggest that the surface micro-structure of TNOs and Centaurs must be very different from that of the small bodies in the inner part of the Solar System.

5 Planet moons

5.1 The Earth's Moon

Our Moon has been polarimetrically studied at a large extent. It was the first object of astrophysical interest observed in polarimetric mode (Arago 1858, [93]), and the object where the phenomenon of negative polarization was first observed (by Lyot 1929, [13]). Many modern polarimetric studies of the Moon are due to Dollfus (e.g., Dollfus 1957, [94], Dollfus 1961, [95]). Gehrels et al. (1964, [12]) obtained multi-colour polarimetric measurements of various regions of the Moon, and recognised the importance of combining polarimetric data with photometric measurements. Later, Dollfus et al. (1971 [96]) showed that for lunar regions polarization and reflectance spectra obey the Umov law, i.e., the polarization and the inverse of the reflectance correlate positively. The Moon is the object of our Solar System that can be investigated with the greatest spatial resolution and in the phase-angle range from nearly 0° to 180°. It is possible to obtain polarimetric maps of the lunar surface through broadband filters, which, combined with colour maps, may be used, e.g., to estimate the average size of regolith particles and their optical inhomogeneity. However, also spectro-polarimetric observations of distinct lunar regions may be of great interest. Opanasenko & Shkuratov (1994, [97]) have suggested that spectro-polarimetry of the Moon may be used to detect weak bands of some minerals (e.g. those of the Cr^3 ion at 625 nm), which in the reflectance spectra would be hidden by the solar spectrum features. Reflectance spectra are obtained after the division by a solar spectrum analogue, but usually the solar spectrum features may not be removed with the necessary accuracy. By contrast, spectropolarimetric measurements are not affected by the solar spectrum (except that solar spectral lines may decrease the S/N ratio at certain wavelengths). Due to the Umov effect, spectropolarimetric data may show more clearly features of the spectral albedo. However, no such weak features have been detected by Opanasenko & Shkuratov (1994, [97]). Bagnulo et al. (2015, [25]) have used their new spectropolarimetric lunar measurements to show that the polarimetric gradient is different from that of asteroids, e.g., steeper than that of S type asteroids. Polarimetric studies of our Moon have been recently reviewed by Shkuratov et al. (2011, [98] and Shkuratov et al. (2015, [99]) to which we address the reader.

Broadband polarization (Dollfus 1957, [94], Bazzon et al. 2013, [100] and spectropolarimetric data (Sterzik et al. 2012, [101], Takahashi et al. 2013 [102] Miles-Páez et al. 2014, [103]) exist also for the Earthshine, but, although by depolarising the radiation lunar regoliths leave their inprint, Earthshine measurements should be regarded as polarimetric measurements of major planets and their atmospheres, hence they are outside of the scope of this paper.

5.2 The moons of the giant planets

Broadband polarimetric observations exist of the Galilean moons, the Saturn moons Enceladus, Rhea, Thetys and Iapetus (for which there are also spectro-polarimetric data), and Uranus moons Ariel, Umbriel, Titania and Oberon. For a full reference list, but also for a recent extensive review, see Rosenbush et al. (2015, [89]). Observations of the planetary moons have a special peculiarity that distinguish them from the observations of asteroids. Most satellites keep the same side directed toward their primary body (including the Earth's Moon). When observed from Earth, during half of their orbit around the planet they show their leading hemisphere, and during the other half they show their trailing hemisphere. Therefore their polarimetrics0. properties may be different at eastern and western elongations. For instance, Ejeta et al. (2012, [104]) and Ejeta et al. 2013a, [105]) presented spectropolarimetric measurements for the bright (trailing) hemisphere of the Saturn moon Iapetus, and for its dark (leading) hemisphere, respectively, over a phase-angle range between 0° and 6°. They found that the two hemispheres showed opposite trend in phase-angle dependence: the linear polarization of Iapetus leading side increases (in absolute terms) as phase-angle increases, reaching $P_{\rm r} = 1.30\,\%$ at $\alpha \simeq 6.0°$, while the polarization of the trailing side tends to slightly decreases with phase-angles and, in absolute value, is three times smaller than that of the leading side – these recent results are in agreement with previous broadband polarization measurements by Zellner (1972, [106]) and Veverka (1977, [107]). Modelling results by Ejeta et al. (2013b, [108]) suggest a geometric albedo values of $\simeq 0.40$ and $\simeq 0.10$ for the trailing and the leading side, respectively. Ejeta et al. (2013b, [108]) found also that variation in polarization of Iapetus two hemispheres with wavelength is in general very small, and found no evidence of detectable circular polarization.

Polarization opposition effects (see Sect. 3.2) were observed in the Jupiter Galilean satellites Io, Europa and Callisto by Rosenbush & Kiselev (2005, [109]) and Kiselev et al. (2009, [110]) in form of a strong and narrow minimum of the (negative) polarization in an otherwise relatively flat branch of negative polarization.

Rosenbush et al. (2015, [89]) have noted that Uranian satellites exhibit polarimetric characteristics similar to those of small TNOs such as Ixion and Huya, reaching very high (in absolute value) polarization at very small phase-angles ($P_{\rm r} = -1.7\,\%$ at $\alpha \simeq 2°$).

6 Comets

Polarimetry of comets was recently reviewed by Kiselev et al. (2015, [111]). Here we briefly summarize the results of cometary polarimetry.

Modern ideas about origin of comets suppose that the comets come from the regions beyond Neptune, namely the Kuiper Belt, the scattered disk and the Oort cloud (e.g., Duncan 2008, [112]). Thus, we can expect that cometary nuclei should be similar to trans-Neptunian objects. However, we do not see a lot of similarity in photopolarimetric characteristics of TNOs and cometary nuclei. As it was mentioned above, polarimetrically, cometary nuclei are more close to F-type asteroids. This is not a big surprise as all comets for which the nuclei were observed were either Jupiter family comets (2P/Encke, Boehnhardt et al. 2008, [59], 67P/Churyumov-Gerasimenko, 74P/Smirnova-Chernykh and 152P/Helin-Lawrence, Stinson et al. 2016, [60]) or main-belt comets (133P/Elst-Pizarro, Bagnulo et al. 2010, [61]). Due to their proximity to the Sun, these objects have highly processed surfaces characterized by lack of volatiles, caused by their sublimation from the surface, and changes produced by the bombardment by charged solar wind particles. We know that cometary surfaces have albedo as low as $\sim 4\,\%$ that, again, tells us that most likely the processing transformed their surfaces to the surfaces similar to those of dark F-type asteroids. Unfortunately, nothing else about cometary nuclei can be currently concluded.

Much more promising is polarimetry of comet comae, as it provides information about size, composition and other properties of the dust particles that are lifted to the coma by sublimating gases or ejected from active areas. Probably, the most impressive result of cometary polarimetry is how much the phase angle dependence of cometary polarization reminds the one for other small bodies, e.g., asteroids or the Moon. It also demonstrates negative polarization for phase angles $\leq 22^\circ$ (similar to asteroids) with $P_{\rm min} = -1.5\,\%$ around 10° (similar to C-type asteroids), and then a bell-shaped branch of positive polarization. However, although qualitatively the cometary positive branch is similar to the asteroidal one, it differs in the location of the maximum (at $90^\circ - 95^\circ$ for comets and $> 100^\circ$ for asteroids and the Moon) and values of maximum positive polarization. The values of maximum polarization deserve a separate consideration as comets may be grouped into two distinct classes, one with lower ($\sim 15\,\%$) and one with higher ($\sim 25-30\,\%$) polarization maximum (these numbers refer to the red spectral domain). We note that comet Hale-Bopp was observed only up to phase-angle 47°, but that in this range shows polarization greater than any other comet. One may expect that its $P_{\rm max}$ value also exceeds the values ever observed for other comets, in which case there would be a third class of comets, with even higher $P_{\rm max}$, which is currently only represented by comet Hale-Bopp (Hadamcik & Levasseur-Regourd 2003, [113]). Note that asteroidal maximum polarization measured so far was below $10\,\%$ with the highest value for C-type asteroids, and lower value, $\sim 7\,\%$, for S-type asteroids and $\sim 2\,\%$ for E-type asteroids. The low values of asteroidal polarization are, most likely, explained by depolarizing effect of multiple scattering discussed above (Kiselev et al.(2002, [114]). In the case of comets, the lower polarization is most likely result of a gas contamination, and the actual values of polarization for cometary dust are $\sim 30\,\%$ (Kolokolova et al. 2007, [115]). This is confirmed by studies of polarimetric images of comets, which show that all comets have high positive polarization near their nucleus; however, for comets with large gas/dust ratio polarization gradually decreases with the distance from the nucleus, whereas for comets with low gas/dust ratio it keeps almost the same values throughout the coma.

The spectral dependence of the cometary polarization is similar to those of low-albedo asteroids Kiselev et al. (2002, [114]), i.e., the gradient is always positive (in other words, in the negative branch, the absolute value of the cometary negative polarization decreases with wavelength, while in the positive branch the absolute value of the polarization increases with wavelength.)

The specifics of cometary polarization is defined by properties of scattering particles and their single-scattering characteristics, whereas in the case of asteroids, the characteristics of the whole regolith layer and multiple scattering in it define the polarimetric characteristics. It was shown repeatedly that simple models like polydisperse spherical (or spheroidal, or cylindrical) particles can reproduce cometary polarization, however they fail when the whole scope of photopolarimetric data (phase and spectral dependence of polarization and phase and spectral dependence of brightness, including albedo) are attempted to be reproduced. The only model capable to reproduce all observational characteristics of comets in both experimental and theoretical modeling was a model of composite, aggregated particles. This model allowed to reproduce cometary data not only in the visible spectral range but also in the near infrared (Kolokolova & Mackowski (2012, [44]) and is consistent with the cosmogonic views on cometesimals formation and available samples of cometary dust particles. The aggregated model of the cometary dust has been confirmed by recent in situ studies by the Rosetta mission, see, e.g., Langevin et al. (2016, [116]), and Bentley et al. (2016, [117]).

6.1 Circular polarization in comets

An outstanding problem in cometary polarimetry is the problem of circular polarization. To the date, it was observed in 11 comets and showed values up to $0.8\,\%$ by Kieselev, Rosenbush and collaborators. Circular polarization of both signs was observed, but negative (left-handed) polarization highly dominates (Kiselev et al. 2015, [111]), which makes the interpretation of this phenomenon particularly problematic. Recent observations of several comets using SCORPIO-2

focal reducer at the 6-m BTA telescope of the Special Astrophysical Observatory (Russia) allowed producing maps of circular polarization in the comet continuum filter at 684 nm and red wide-band filter (Kiselev et al. 2013, [118]). A gradual increase of the circular polarization with the nucleocentric distance was usually observed, and several mechanisms have been suggested to explain the data. The most often suggested mechanisms of formation of circular polarization are multiple scattering of light in asymmetric medium and alignment of dust particles. However, multiple scattering could not be responsible for cometary circular polarization due to a low number density of dust in the coma that usually produces optical thicknesses much smaller than unity. The alignment of the dust particles looks more realistic as it was already detected in cometary coma it is considered the mechanism responsible for non-zero polarization at stellar occultation (Rosenbush et al. 1994, [119]). However, all mechanisms of the alignment face some difficulties. Gas drag could align the particles only very close to the nucleus, and then the alignment quickly should be destroyed by radiative torque. Radiative torque could not produce circular polarization as it aligns particles by the long axis perpendicular to the source of light and, thus after azimuthal averaging should produce zero circular polarization. Homochirality of cometary organic molecules was also considered as a possible cause of cometary circular polarization, however, the amount of such organics in the cometary dust particles is too small to produce any noticeable effect (Sparks et al. 2015, [120]). Alignment in the solar magnetic field was one of the first mechanisms suggested to explain cometary circular polarization (Dolginov and Mytrophanov 1976 ,[121]; 1978, [122]). For a long time this mechanism was considered as doubtful, because in situ data for comet Halley showed that the solar magnetic field does not penetrate deep into the coma and cannot be responsible for the polarization observed closer than 2-5000 km from the nucleus (Neubauer et al. 1986, [123]). However, recent developments of the theory of interaction of the cometary ions with the solar magnetic field and, especially, the data on the near-nucleus magnetic field of comet 67P/Churyumov-Gerasimenko obtained by the Rosetta mission, showed that it is very likely to have the dust aligned by the solar magnetic field very close to the nucleus, and, thus, to explain the observations of the cometary circular polarization, including its observations close to the nucleus and increase of the circular polarization with the distance from the nucleus; for details see Kolokolova et al. (2016, [124]).

We note that cross-talk from linear to circular polarization is a problem very difficult to avoid, hence any claim of detection of circular polarization in highly linearly polarized objects such as comets should be supported by an accurate instrument characterization. At the very least, observations of circular polarization should be repeated with the instrument position angle on sky rotated by 90°. Equations (2) show that P_Q and P_U would reverse their sign, and so should do any effect of cross-talk from linear polarization. By contrast, a circular polarization signal intrinsic to the source would remain independent of the instrument position angle.

7 Conclusions

In planetary science, as with many other research areas, it is important to recognise that the radiation is not only described by its intensity as a function of wavelength and time, but by all four Stokes parameters, which all together describe also how photons oscillate in the plane perpendicular to the direction of propagation. In many cases, intensity and linear polarization measurements have a diagnostic content by far superior to what obtained from intensity measurements alone.

It is thanks to the use of different observing techniques that we can make important progresses in the physical characterization of small bodies and satellites. In particular, a stronger synergy of polarimetry, thermal radiometry and visible photometry will be of the highest importance.

References

1. Bagnulo, S., Belskaya, I., Muinonen, K., Tozzi, G.P., Barucci, M.A., Kolokolova, L., & Fornasier, S. 2008, A&A, 491, L33
2. Landi Degl'Innocenti, E., Bagnulo, S., Fossati, L. 2007, in: The Future of Photometric, Spectrophotometric and Polarimetric Standardization, ASP Conference Series, 364, 495
3. Boehnhardt H., Bagnulo S., Muinonen K., Barucci, M.A., Kolokolova, L., Dotto, E., and Tozzi, G.P. 2004, A&A, 415, L21
4. Breger, M., & Cochran, W. D. 1982, Icarus, 49, 120
5. Zellner, B., Gehrels, T. & Gradie, J. 1974, AJ, 79, 1100
6. Zellner, B., & Gradie, J. 1976, Icarus, 28, 117
7. Fornasier, S., Belskaya, I.N., Shkuratov, Yu.G., Pernechele, C., Barbieri, C., Giro, E., & Navasardyan, H. 2006, A&A, 445, 371
8. Gil-Hutton, R., Cellino, A. & Bendjoya, Ph. 2014, A&A, 569, A122
9. Manset, N. & Bastien, P. 2000, Icarus, 145, 203
10. Ganesh, S., Joshi, U. C., Baliyan, K.S., & Deshpande, M. R. 1998, A&AS, 129, 489
11. Chernova, G.P., Kiselev, N.N., & Jockers, K. 1993, Icarus, 103, 144
12. Gehrels, T., Coffeen, T., & Owings, D. 1964, AJ, 69, 826

13. Lyot, B. 1929, Ann. Obs. Paris, vol. 8, 1
14. Mukai, T., Mukai, S., & Kikuchi, S. 1987, A&A, 187, 650
15. Lumme, K., & Muinonen, K. 1993, IAU 160, 194
16. Penttilä, A., Lumme, K., Hadamcik, E., Levasseur-Regourd, A.-C. 2005, A&A, 432, 1081
17. Kaasalainen, S., Piironen, J., Kaasalainen, M., Harris, A.W., Muinonen, K, & Cellino, A. 2003, Icarus, 161, 34
18. Cellino, A., Bagnulo, S., Gil-Hutton, R., Tanga, P., & Cañada-Assandri, M. 2015a, MNRAS, 451, 3473
19. Beuzit, J.-L., Feldt, M., Dohlen, K., et al. 2008, SPIE, 7014, 701418
20. Thalmann, C., Schmid, H.M., Boccaletti, A., et al. 2008, SPIE, 7014, 70143F
21. Kolokolova, L., & Kimura, H. 2010, A&A, 513, A40
22. Kolokolova, L., Hanner, M., Levasseur-Regourd, A.-Ch., & Gustafson, B.Å.S. 2004. In Comets II, M.C. Festou, H.U. Keller, & H.A. Weaver (eds.), University of Arizona Press, p. 577.
23. Lupishko, D.F., & Kiselev, N.N., 1995, Bull. Am. Astron. Soc. 27, 1064.
24. Belskaya, I.N., Levasseur-Regourd, A.C., Cellino, A., Efimov, Yu, S., Shakhovskoy, N.M.,Hadamcik, E. & Bendjoya, Ph. 2009a, Icarus, 199, 97
25. Bagnulo, S., Cellino, A. & Sterzik, M.F. 2015, MNRAS, 446, L11
26. Bagnulo, S., Landolfi, M., Landstreet, J.D., Landi Degl'Innocenti, E., Fossati, L., & Sterzik, M.F. et al. 2009, PASP, 121, 993
27. Appenzeller, I., Fricke, K., Furtig, W., et al. 1998, The Messenger, 94, 1
28. Le Borgne, J.F. & Crovisier, J. 1987, in: ESA, Proceedings of the International Symposium on the Diversity and Similarity of Comets, p. 171
29. Keller, C.U., Snik, F., Harrington, D., & Packhman, C. 2015, in: Polarimetry of Stars and Planetary Systems, L. Kolokolova, Hough, J., & Levasseur-Regourd, A.-C. (eds), Cambdridge University Press, p. 35
30. Pernechele, C., Abe, L., Bendjoya, Ph., Cellino, A., Massone, G., Rivet, J.P., & Tanga, P. 2012, SPIE, 8446, 84462H
31. Devogèle, M., Cellino, A., Bagnulo, S., et al. 2017. MNRAS, 465, 4335.
32. Wiktorowicz, S.J., & Nofi, L.A., 2015, ApJ, 800, L1
33. Bagnulo, S., Belskaya, I.N., Boehnhardt, H., Kolokolova, L., Muinonen, K.,Sterzik, M., & Tozzi G.P. 2011, JQSRT, 112, 2059
34. Bagnulo, S., Belskaya, I., Stinson, A., Christou, A., & Borisov, G.B. 2016, A&A, 585, 122
35. Umov, N. 1905, Physik. Z., 6, 674
36. Wolff, M. 1980, Icarus, 44, 780
37. Wolff, M. 1981, Applied Optics, 20, 2493
38. Kolokolova, L. 1990, Icarus, 84, 305
39. Shkuratov Yu.G., Muinonen, K., Bowell, E., et al. 1994, EM&P, 65, 201
40. Muinonen, K. 1994, in: Asteroids, Comets, Meteors 1993, A. Milani, M. Di Martino, & A. Cellino (eds.), Kluwer Academic Publishers, p. 271
41. Muinonen, K., Penttilä, A., & Videen, G. 2015, in: Polarimetry of Stars and Planetary Systems. L. Kolokolova, J. Hough, A.-C. Levasseur-Regourd (eds.) Cambridge University Press, Cambridge, UK, p. 114
42. Mackowski, D. W., & Mishchenko, M.I. 1996, J. Opt. Soc. Am. A., 13, 2266
43. Draine, B.T., & Flatau, P.J. 1994, J. Opt. Soc. Am. A., Opt. Image Sci. 11, 1491
44. Kolokolova, L., & Mackowski, D.W. 2012, JQSRT, 113, 2567
45. Zubko, E., Muinonen, K., Videen, G., & Kiselev, N. 2014, MNRAS, 440, 2928
46. Dollfus, A., & Zellner, B. 1979, in: Asteroids I, University of Arizona Press, p. 170
47. Masiero, J.R., Mainzer, A.K., Grav., T., et al. 2011, ApJ, 741, 66
48. Cellino, A., Gil-Hutton, R., & Belskaya, I.N. 2015b, in: Polarimetry of stars and planetary systems, L. Kolokolova, J. Hough, A.-C. Levasseur-Regourd, (eds.), Cambridge University Press, Cambridge, UK, p.360
49. Zellner, B., Leake, M., Lebertre, T., Duseaux, M., & Dollfus, A. 1977, Proc. Lunar Sci. Conf. 8th, p. 1091
50. Shevchenko, V.G., & Tedesco, E.F. 2006, Icarus, 184, 211
51. Rosenbush, V.K., Kiselev, N.N. & Shevchenko, V.G. 2005, Icarus, 178, 222
52. Rosenbush, V.K., Shevchenko, V.G. & Kiselev, N.N. 2009, Icarus, 201, 655
53. Bus, S. J., & Binzel, R.P. 2002, Icarus, 158, 146
54. DeMeo, F., Binzel, R.P., Slivan, S.M., Bus, S.J. 2009, Icarus, 202, 160.
55. Belskaya I.N., Fornasier S., Tozzi G. P., Gil-Hutton R., Cellino A., Antonyuk K., Krugly Yu. N., Dovgopol A. N., Faggi S. 2017. Icarus, 284, 30
56. Gradie, J. & Tedesco, E. F. 1982, Science, 216, 1405
57. Belskaya, I.N., Shkuratov, Yu. G., Efimov, Yu. S., et al. 2005, Icarus, 178, 213
58. Chamberlin, A.B., McFadden, L.-A., Schulz, R., Schleicher, D.G., & Bus, S. J. 1996, Icarus, 119, 173
59. Boehnhardt, H., Tozzi, G.P., Bagnulo, S., Muinonen, K., Nathues, A., & Kolokolova, L. 2008, A&A, 489, 1337
60. Stinson, A., Bagnulo, S., Tozzi, G.P., et al. 2016, A&A, 594, A110
61. Bagnulo, S., Tozzi, G.P., Boehnhardt, H., Vincent, J.-B., & and Muinonen, K. 2010, A&A, 514, A99
62. Cellino, A., Belskaya, I.N., Bendjoya, Ph., Di Martino, M., Gil-Hutton, R., Muinonen, K., & Tedesco, E.F. 2006, Icarus, 180, 565
63. Gil-Hutton, R., Mesa, V., Cellino, A., Bendjoya, Ph., Peñaloza, L., Lovos, F. 2008, A&A, 482, 309
64. Masiero, J. & Cellino, A. 2009, Icarus, 199, 333

65. Sunshine, J.M., Connolly, H.C., McCoy, T.J., Bus, S.J., La Croix, L.M. 2008, Science, 320, 514
66. Cellino, A., Bagnulo, S., Tanga, P., Novaković, B., & Delbò, M. 2014, MNRAS, 439, L75
67. Bottke, W. F., Jr., Vokrouhlický, D., Rubincam, D.P., & Broz, M. 2002, in: Asteroids III, W. F. Bottke Jr., A. Cellino, P. Paolicchi, & R. P. Binzel (eds.), University of Arizona Press, Tucson, p. 395
68. Wetherill, G.W., 1975, in: Lunar Sci. Conf. 6th, Proceedings. Volume 2. New York, Pergamon Press, Inc., p. 1539
69. De Luise F., Perna D., Dotto E., et al. 2007, Icarus, 191, 628.
70. Belskaya I.N., Fornasier S., & Krugly Yu.N., 2009b, Icarus, 201, 167
71. Belskaya, I.N., Cellino, A., Gil-Hutton, R. et al. 2015, Asteroids IV, p.151, Univ. of Arizona Press, Tucson
72. Fornasier, S., Belskaya, I.N., & Perna, D. 2015, Icarus, 250, 280
73. Lupishko, D. (Ed.) 2014, Asteroid Polarimetric Database V8.0. EAR-A-3-RDR-APDPOLARIMETRY- V8.0. NASA Planetary Data System
74. Dollfus A., Wolff, M., Geake, J.E., Lupishko, D.F. & Dougherty L.M. 1989. In: Asteroids II; R.P. Binzel, T. Gehrels, M.S. Matthews, (eds.), University of Arizona Press, Tucson, AZ, p. 594
75. Sierks, H., Lamy, P., Barbieri, C. et al. 2011, Science, 334, 487
76. Belskaya, I.N., Fornasier, S., Krugly, Yu.N., Shevchenko, V.G., Gaftonyuk, N.M., Barucci, M.A., Fulchignoni, M., & Gil-Hutton, R. 2010b, A&A, 515, 29
77. Farnham, T.L., 2013, Shape model of asteroid 21 Lutetia, RO-A-OSINAC/OSIWAC-5-LUTETIA-SHAPE-V1.0, Planetary Data System
78. Keihm, S., Tosi, F., Kamp, L., et al. 2012, Icarus, 221, 395
79. Lamy, P.L., Groussin, O., Fornasier, S., Jorda, L., Kaasalainen, M., & Barucci, M.A. 2010, A&A, 516, 74
80. Coradini, A., Capaccioni, F., Erard, S., et al. 2011, Science, 334, 492
81. Tanga, P., Carry, B., Delbò, M., et al. 2015, MNRAS, 448, 3382
82. Kelsey, J. D., and Fix, L. A. 1973, AJ, 184, 633
83. Avramchuk, V. V., Rakhimov, V. Iu., Chernova, G. P., & Shavlovskii, V.I. 1992 Kinematics Phys. Celest. Bodies, 8, 30
84. Emery, J.P., Marzari, F., Morbidelli, A., French, L.M., & Grav, T. 2015, in: Asteroid IV, P. Michel, F.E. DeMeo, & W.F. Bottke Jr. (eds.). The University of Arizona Press, in press (arXiv:1506.01658)
85. Belskaya, I.N., Bagnulo, S., Barucci, M.A., Muinonen, K., Tozzi, G.P., Fornasier, S., & Kolokolova, L. 2010a, Icarus, 210, 472
86. Belskaya, I.N., Bagnulo, S., Stinson, A., Tozzi, G.P., Muinonen, K., Shkuratov, Yu.G., Barucci, M.A., & Fornasier, S. 2012, A&A, 547, A101
87. Bagnulo, S., Boehnhardt, H., Muinonen, K., Kolokolova, L., Belskaya, I.,& Barucci, M.A. 2006. A&A, 450, 1239
88. Belskaya, I., Bagnulo, S., Muinonen, K., Barucci, M.A., Tozzi, G.P., Fornasier, S., & Kolokolova, L. 2008a, A&A, 479, 265
89. Rosenbush, V., Kiselev, N., & Afanasiev, V. 2015, in: Polarimetry of Stars and Planetary Systems. L. Kolokolova, J. Hough, A.-C. Levasseur-Regourd (eds.) Cambridge University Press, Cambridge, UK, p. 340
90. Rousselot, P., Levasseur-Regourd, A.C., Muinonen, K., & Petit, J.-M. 2005, Earth, Moon,& Planets, 97, 353
91. Shkuratov Yu.G., Ovcharenko A., Zubko E., et al. 2002, Icarus, 159, 396
92. Dougherty, I.M., & Geake, J.E. 1994, MNRAS, 271, 343
93. Arago, F. 1858, Les Comètes. Paris: Gide Editeur
94. Dollfus, A. 1957, Supplements aux Annales d'Astrophysique, 4, 3
95. Dollfus, A. 1961, in: Planets and satellites, P. Kuiper & B.M. Middlehurst (eds.) University of Chicago Press, Chicago, Chapter 9
96. Dollfus, A., Bowell, E., & Titulaer, C. 1971, A&A, 10, 450
97. Opanasenko, N. V. & Shkuratov, Y. G. 1994, Solar System Research, 28, 398
98. Shkuratov Yu.G., Kaydash V., Korokhin V. et al. 2011, Planetary and Space Science, 59, 1326
99. Shkuratov Yu.G., Opanasenko, N., Korokhin V., & Videen, G. 2015, in: Polarimetry of Stars and Planetary Systems, L. Kolokolova, Hough, J., & Levasseur-Regourd, A.-C. (eds), Cambdridge University Press, p. 303
100. Bazzon, A., Schmid, H. M., & Gisler, D. 2013, A&A 556, 117
101. Sterzik, M., Bagnulo, S., & Pallé, E. 2012, Nature, 483, 64
102. Takahashi, J., Itoh, Y., Akitaya, H., Okazaki, A., Kawabata, K., Oasa, Y., Isogai, M. 2013, PASJ, 65, 38
103. Miles-Páez, P. A., Pallé, E., & Zapatero Osorio, M. R. 2014, A&A, 562, L5
104. Ejeta, C., Boehnhardt, H., Bagnulo, S., & Tozzi, G. P. 2012, A&A, 537, 23
105. Ejeta, C.T., Boehnhardt, H., Bagnulo, S., Muinonen, K., Kolokolova, L., & Tozzi, G. 2013a, A&A, 549, 61
106. Zellner, B.H. 1972, ApJ, 174, L107
107. Veverka, J., 1977, in: Planetary Satellites. J.A. Burns (ed.), Tucson: University of Arizona Press, pp. 210
108. Ejeta, C., Muinonen, K., Boehnhardt, H., Bagnulo, S., Kolokolova, L., Guirado, D., & Tozzi, G.P. 2013b, A&A, 554, 117
109. Rosenbush, V.K., & Kiselev, N.N. 2005, Icarus, 179, 490
110. Kiselev, N., Rosenbush, V., Velichko, F., & Zaitsev, S. 2009, JQSRT, 110, 1713
111. Kiselev, N., Rosenbush, V., Kolokolova, L., & Levasseur-Regourd, A.-Ch 2015, in: Polarimetry of Stars and Planetary Systems, L. Kolokolova, Hough, J., & Levasseur-Regourd, A.-C. (eds), Cambdridge University Press, p. 379
112. Duncan, M. J. 2008, Space Science Reviews, 138, 109
113. Hadamcik, E., & Lavasseur-Regourd, A. 2003, JSQRT, 79, 661
114. Kiselev, N.N., Kiselev, N.N., Rosenbush, V.K., Petrova, E. V., & Jockers, K. 2002, Memorie della Societa Astronomica Italiana, 73, 703.

115. Kolokolova, L., Kimura, H., Kiselev, N., & Rosenbush, V. 2007, A&A, 463, 1189
116. Langevin, Y., Hilchenbach, M., Ligier, N., et al. 2016, Icarus, 271, 76
117. Bentley, M.S., Schmied, R., Mannel, T., et al. 2016, Nature, 537, 73
118. Kiselev, N.N., Rosenbush, V.K., Afanasiev, V.L., Kolesnikov, S.V., Zaitsev, S.V., & Shakhovskoy, D.N. 2013, Earth, Planets and Space, 65, 1151
119. Rosenbush, V.K., Rosenbush, A.E., & Dementev, M.S. 1994, Icarus, 108, 81
120. Sparks, W., Hough, J., Kolokolova, L. 2015, in: Polarimetry of Stars and Planetary Systems, L. Kolokolova, Hough, J., & Levasseur-Regourd, A.-C. (eds), Cambdridge University Press, p. 462
121. Dolginov A. Z., Mytrophanov I. G., 1976, Ap&SS , 43, 291
122. Dolginov A. Z., Mytrophanov I. G., 1978, A&A , 69, 421
123. Neubauer, F.M., Glassmeier, K.H., Pohl, M., et al. 1986, Nature, 321, 352
124. Kolokolova, L., Koenders, C., Goetz, C., Rosenbush, V., Kiselev, N., Hoang, T. and Lazarian, A., 2016, MNRAS, 462, S422